16th AIMMS-MOPTA Optimization Modelling Competition Report

Bárbara Rodrigues Daniel Kopisitskiy Denise Cariaga Sandoval

August 10, 2024

Executive Summary

In this report, we present our solution to the 16th AIMMS-MOPTA Optimization Modeling Competition on whether a fully renewable energy grid would benefit from adding green hydrogen as a supplemental flexible source to power generation.

We propose a two-stage stochastic optimization model where investment decisions in renewable plants and hydrogen storage are minimized in the first stage, and operational costs of running the hydrogen storage systems in the second stage. This model accounts for uncertainties in both solar and wind generation.

All in all, the results in this report show that there is potential for green hydrogen as a source of baseload support in the transition to a fully renewable-powered energy grid. For the data considered, we see that a fully renewable network driven by green hydrogen has a greater potential to succeed under realities where wind generation is high. In addition, we note that the main driver for the potential and profitability of green hydrogen lies in the electricity demand and prices, as opposed to those for gas. We also conclude that the investment in long-term liquid hydrogen storage is more valuable for taking full advantage of hydrogen as a baseload source than that in shorter-term intraday hydrogen gas storage. Finally, we have seen that our model is robust to changes in the investment costs for the data collected.

For future work, we suggest a further exploration of uncertainties, by using more accurate scenarios for wind and solar generation, or by considering other sources of uncertainty, such as the residential demand patterns or variability of technology investment costs. Lastly, a more extensive long-term analysis of the green hydrogen viability could be carried out by performing further sensibility analyses, and computing the net discounted present value for long-term investments.

This report has the following structure. In Section 1, we describe the motivation of this work on the study of hydrogen storage as a complementary electrical and gas supply source to ensure the viability and resilience of the energy grid. On Section 2, we explain the modeling approach used to formulate the problem, as well as describe the data used and the user interface developed. Then, in Section 3, we present the solution of a minimum non-trivial solution, analyze the economics of the loss of load, discuss the current viability of green hydrogen, and analyze the robustness of the solution obtained for varying investment cost trends. Finally, the main conclusions and future work are described in Section 4.

1 Motivation

In pursuit of decarbonization goals, it becomes imperative to integrate renewable energy technologies into energy grids at a large scale. However, an important challenge arises concerning the stability of the energy grid's baseload. This baseload stability can not be provided consistently by renewable sources due to their dependence on the weather and uncertain generation. Thus, the transition towards decarbonization needs a departure from coal and natural gas as baseload supporters. This creates the challenge of finding flexible green sources that would allow the power network to work continuously and safely by offering baseload support.

The operation of a fully renewable energy grid needs a reliable energy source and storage to provide a continuous supply of energy to the grid. Green hydrogen emerges as a promising candidate, not only for decarbonizing big industries' gas demand but also for offering baseload power. Stored hydrogen as compressed gas or liquid can either be converted back to electricity or used as feedstock for industry or as fuel for vehicles.

In the remainder of this section, we briefly describe the problem that we propose solving, why it is a relevant problem, and detail some other pieces of work that have studied it.

1.1 Problem Description

In order to study the viability of green hydrogen, we want to find the optimal renewable mix of solar and wind power to be built, such that the electricity and gas demands are met, using hydrogen as a means to store energy in a fully renewable system. In order to achieve this, we assume that relying on electricity from other power sources, such as coal and natural gas, is not a possibility. Therefore, one of the main questions of the problem is how much long- and short-term hydrogen energy storage is needed and how much this set-up will cost.

In our work, we consider an energy grid as presented in Figure 1 with 7 different types of locations: solar and wind plants, hydrogen systems such as electrolyzers, tanks and fuel cells, and industrial and residential demand areas. Solar and wind power plants provide the generation, and they can supply the demand locations, both industry and residential areas, directly or feed into the electrolyzer to convert the electricity into hydrogen gas. Hydrogen gas can be stored for intraday use only. It can used to meet the gas demand in the industry sectors, or it can be liquefied and stored in long-term storage tanks. Later, this liquid hydrogen can be converted back into electricity using the fuel cell to meet demand and offer baseload support.

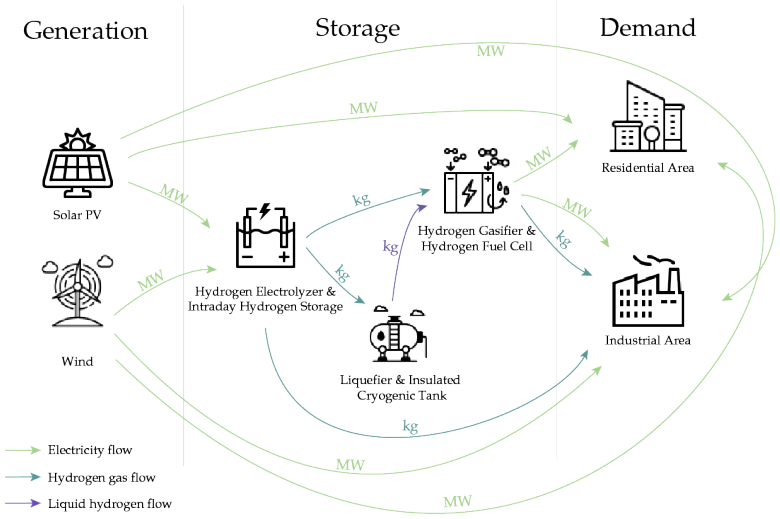

Figure 1: Scheme of the types of locations and energy flows in the network considered.

The goal of the problem is to determine how much electricity needs to be injected into the energy grid to meet demand during a given period. It is essential that the electricity and gas demand is matched precisely with the supply, as deviations from this could severely damage the

grid infrastructure or cause blackouts. For this, an optimization model was used to solve the problem whilst incorporating all the features of an integrated and fully renewable energy system, for both gas and electricity simultaneously, as green hydrogen can be a source of either.

1.2 Background

As previously mentioned, hydrogen energy storage systems can help renewable energy sources overcome the challenges associated with higher penetrations of wind and solar power [15, 17]. In periods of excess generation, electricity can be converted into green hydrogen and stored as a compressed gas or liquid for later use. The hydrogen stored can be converted back into electricity in times of supply shortage [11, 19]. Especially for tactical decisions that span multiple days, weeks, or months, as is the case for this study, hydrogen storage can be attractive.

The efficiency of the hydrogen conversion from and to electricity is one of the drawbacks of this technology. For example, the electrolyzer efficiency varies with input power, and according to [4], it should be operated with constant input power corresponding to max efficiency to minimize losses. Also, even though there is almost no loss of stored hydrogen, the total energy loss in a hydrogen system used for storing electricity is substantial, in particular when compared to battery systems. The authors explain that typical efficiencies for electrolyzers are in the range of 60–80%, and typical efficiencies for fuel cells are in the range of 40–60%. In summary, around 54 to 72% of electric energy is lost in the electrolyzer and fuel cell combined, and in addition to this, you lose about 20% of the energy if hydrogen is stored as high-pressure gas, and 25–45% if it is stored as liquid hydrogen. Therefore, these concerns should be taken into account in future work.

Furthermore, the authors propose a solution for the loss of efficiency: a hybrid energy storage system where hydrogen storage is combined with batteries and supercapacitors as a possible third component to handle extremely rapid and large power fluctuations (if there are any). Since batteries are very suitable for short-term energy storage and hydrogen for long-term storage, the two technologies combine well in a system where batteries can deal with high-frequency fluctuations in power demand and hydrogen handles the remaining low-frequency fluctuations [4].

On the other hand, an investment model with uncertain information, like the renewable generation in this case, is normally approached using a two-stage stochastic model, where the first stage minimizes the investment decisions and the second stage deals with the operational side of the problem [10, 12]. There are some works that use this technique for hydrogen storage. Namely, the authors in [7] take the investment decisions in the first stage, and operational decisions for minimizing CO2 emissions in the second. In [14], a risk-averse two-stage stochastic model is used, with the decisions on transactions with bilateral electrical contracts as the first-stage decision variables and the other decision variables taken in the second stage, using uncertain demand and electricity prices in the day-ahead market.

2 Our Approach

In this section, we detail the formulation developed to tackle this problem, detail how the data input used in our computational experiments was created, and how our user interface can be used to further study the potential of green hydrogen for different realities.

2.1 Modelling Approach

In order to study the problem described in Section 1.1, we developed a 2-stage stochastic mixed-integer linear optimization program. We have chosen a stochastic model to account for the uncertainties in renewable generation and opted for a 2-stage model to capture both the impact of the strategic investment decisions and of the operational grid flows on the total costs.

Below, we briefly introduce the optimization model that was developed. A complete list of the notation used, the corresponding description, and units can be found in Appendix A. In red, the first-stage investment variables are displayed, and in blue, the second-stage operational variables are presented. First, in the objective function, we minimize the first-stage investment costs in

renewable plants and storage technologies:

$$\sum_{i\in\mathcal{V}^S} B_i^S b_i^S + \sum_{i\in\mathcal{V}^W} B_i^W b_i^W + \sum_{i\in\mathcal{V}^E} B_i^G y_i^G + \sum_{i\in\mathcal{V}^T} B_i^L y_i^L \tag{1}$$

as well as the second-stage expected operational costs for using the available storage:

$$\sum_{s\in\mathcal{S}} w_s \left(\sum_{\substack{i\in\mathcal{V}^E \\ t\in\mathcal{T}}} C^G s_{i,t,s}^G + \sum_{\substack{i\in\mathcal{V}^T \\ t\in\mathcal{T}}} C^L s_{i,t,s}^L \right) \tag{2}$$

where b_i^S (respectively b_i^W) is the number of rows of solar plants (resp. wind turbines) to be built at candidate location i where a solar (resp. wind) plant can be built. The parameters B_i^S and B_i^W are the associated costs of building a row of solar panels and wind turbines, respectively. Similarly, the variables y_i^G and y_i^L denote the number of intraday gas storage tanks and of long-term liquid hydrogen tanks to be built, respectively, and B_i^G and B_i^L the associated investment costs. In the second-stage objective term, we consider an average of operation cost weighted on each renewable generation scenario $s \in \mathcal{S}$ according to the weight w_s. The operational costs account for the cost of storage, where $s_{i,t,s}^G$ and $s_{i,t,s}^L$ are the amount of hydrogen gas and liquid hydrogen stored at location i, at time period t, respectively, and C^G and C^L are the associate costs.

Most of our constraints concern flow balance equations that ensure a feasible flow of electricity and gas through the energy grid under all generation scenarios over the time horizon considered. In particular, these flows ensure that the demand of residential and industrial areas is met in a way that guarantees the loss of load doesn't exceed a maximum as:

$$\sum_{j\in\mathcal{V}} f_{j,i,t,s}^E = D_{i,t}^E - u_{i,t,s}^E \qquad \forall i \in \mathcal{V}^I \cup \mathcal{V}^R, t \in \mathcal{T}, s \in \mathcal{S} \tag{3}$$

$$\sum_{j\in\mathcal{V}} f_{j,i,t,s}^G = D_{i,t}^G - u_{i,t,s}^G \qquad \forall i \in i \in \mathcal{V}^I, t \in \mathcal{T}, s \in \mathcal{S} \tag{4}$$

$$\sum_{\substack{i\in\mathcal{V}^I \bigcup \mathcal{V}^R \\ t\in\mathcal{T}}} u_{i,t,s}^E \leq L^E \left(\sum_{\substack{i\in\mathcal{V}^I \bigcup \mathcal{V}^R \\ t\in\mathcal{T}}} D_{i,t}^E \right) \qquad \forall s \in \mathcal{S} \tag{5}$$

$$\sum_{\substack{i\in\mathcal{V}^I \\ t\in\mathcal{T}}} u_{i,t,s}^G \leq L^G \left(\sum_{\substack{i\in\mathcal{V}^I \\ t\in\mathcal{T}}} D_{i,t}^G \right) \qquad \forall s \in \mathcal{S} \tag{6}$$

where constraints (3) and (4) ensure that the electricity and gas that flows into demand areas meets the electricity demand $D_{i,t}^E$ and the gas demand $D_{i,t}^G$, respectively. These equations allow for losing electricity and gas demand through the loss of load variables $u_{i,t,s}^E$ and $u_{i,t,s}^G$, respectively. Constraints (5) and (6) ensure that the percentage of loss of load does not exceed L^E and L^G for electricity and gas, respectively.

Furthermore, we consider flow balance for the other types of locations in our network, namely renewable plants (Equation (7)), electrolyzers (Equation (8)), liquid hydrogen tanks (Equation (9)), and fuel cells (Equation (10)).

$$G_{i,t,s}^S b_i^S + G_{i,t,s}^W b_i^W = \sum_{j\in\mathcal{V}} f_{i,j,t,s}^E + a_{i,t,s} \qquad \forall i \in \mathcal{V}^S \cup \mathcal{V}^W, t \in \mathcal{T}, s \in \mathcal{S} \tag{7}$$

$$\sum_{j\in\mathcal{V}} f_{j,i,t,s}^E = \eta_i^E U^{EG} \left(\sum_{j\in\mathcal{V}} f_{i,j,t,s}^G + c_{i,t,s}^G - d_{i,t,s}^G \right) \qquad \forall i \in \mathcal{V}^E, t \in \mathcal{T}, s \in \mathcal{S} \tag{8}$$

$$\sum_{j\in\mathcal{V}} f_{j,i,t,s}^G = \eta_i^T U^{GL} \left(\sum_{j\in\mathcal{V}} f_{i,j,t,s}^L + c_{i,t,s}^L - d_{i,t,s}^L \right) \qquad \forall i \in \mathcal{V}^T, t \in \mathcal{T}, s \in \mathcal{S} \tag{9}$$

$$\eta_i^F \left(\sum_{j \in \mathcal{V}} f^G_{j,i,t,s} + U^{GL} \sum_{j \in \mathcal{V}} f^L_{j,i,t,s} \right) = \sum_{j \in \mathcal{V}} f^G_{i,j,t,s} + \frac{1}{U^{EG}} \sum_{j \in \mathcal{V}} f^E_{i,j,t,s} \quad \forall i \in \mathcal{V}^F, t \in \mathcal{T}, s \in \mathcal{S} \tag{10}$$

where $f^E_{i,j,t,s}$, $f^G_{j,i,t,s}$ and $f^L_{i,j,t,s}$ represent the flow of electricity, hydrogen gas and liquid hydrogen between locations i and j at time period t under scenario s, respectively.

In constraint (7), we ensure that the solar $G^S_{i,t,s}$ and wind $G^W_{i,t,s}$ electricity generated scaled to the installed capacity (b^S_i and b^W_i) flows into any of the locations connected to the renewable plants or is spilled ($a_{i,t,s}$).

Constraint (8) states that each unit of electricity that flows into an electrolyzer is converted into U^{EG} units of hydrogen gas, and this electrolysis process has an efficiency of η^E_i. Note that here we account for the flows of hydrogen gas going into and out of the intraday gas storage (located at electrolyzer locations) with variables $c^G_{i,t,s}$ and $d^G_{i,t,s}$, respectively.

In an analogous way, constraint (9) ensures that each unit of hydrogen gas that flows into a tank location is converted into U^{GL} units of liquid hydrogen, and this liquefaction process has an efficiency of η^T_i. This is achieved while accounting for the flows of liquid hydrogen being charged and discharged from the hydrogen tank storage with variables $c^L_{i,t,s}$ and $d^L_{i,t,s}$, respectively.

Lastly, in constraint (10), we enforce that the flows of liquid and gas hydrogen going into the fuel cell match the flows of hydrogen gas and electricity going out, where η^F_i is the efficiency of the gasification process.

In addition, we consider constraints (11)-(14) to keep track of the state of charge of the intraday hydrogen gas storage and of long-term hydrogen tanks. These constraints are modeled using the linear DC flow equations.

$$s^G_{i,t,s} = (1 - \alpha^G_i) s^G_{i,t-1,s} + \gamma^G_i c^G_{i,t-1,s} - \frac{d^G_{i,t-1,s}}{\mu^G_i} \quad \forall i \in \mathcal{V}^E, t \in \mathcal{T} \setminus \bigcup_{d \in \mathcal{D}} \{t^I_d\}, s \in \mathcal{S} \tag{11}$$

$$s^G_{i,t^I_d,s} = (1 - \alpha^G_i) s^G_{i,t^F_d,s} + \gamma^G_i c^G_{i,t^F_d,s} - \frac{d^G_{i,t^F_d,s}}{\mu^G_i} \quad \forall i \in \mathcal{V}^E, d \in \mathcal{D}, s \in \mathcal{S} \tag{12}$$

$$s^L_{i,t,s} = (1 - \alpha^L_i) s^L_{i,t-1,s} + \gamma^L_i c^L_{i,t-1,s} - \frac{d^L_{i,t-1,s}}{\mu^L_i} \quad \forall i \in \mathcal{V}^T, t \in \mathcal{T} \setminus \{0\}, s \in \mathcal{S} \tag{13}$$

$$s^L_{i,0,s} = (1 - \alpha^L_i) s^L_{i,|\mathcal{T}|,s} + \gamma^L_i c^L_{i,|\mathcal{T}|,s} - \frac{d^L_{i,|\mathcal{T}|,s}}{\mu^L_i} \quad \forall i \in \mathcal{V}^T, s \in \mathcal{S} \tag{14}$$

where $s^G_{i,t,s}$ and $s^L_{i,t,s}$ represent the state of charge of the gas and liquid hydrogen storage, respectively. The parameters α^G_i, γ^G_i, and μ^G_i are the self-discharge rate and efficiencies of charge and discharge of the gas storage, respectively. Similarly, the parameters α^L_i, γ^L_i, and μ^L_i are the corresponding efficiencies of the liquid tank. Since the gas storage is only for intraday use, constraint (12) ensures that the state of charge at start of time period t^I_d (which is the first period of day $d \in \mathcal{D}$) is the same as that at the end of time period t^F_d (which is the last period of day $d \in \mathcal{D}$). Constraint (14) ensures that the state of charge of the long-term liquid tank is the same at the start and end of the time horizon, a typical restriction used to prevent the model from making use of "free energy".

Finally, we also add constraints to define the domain and bounds of the model's variables.

$$0 \leq b^S_i \leq \bar{P}_i;\ b^S_i \in \mathbb{Z} \quad \forall i \in \mathcal{V}^S \tag{15}$$

$$0 \leq b^W_i \leq \bar{W}_i;\ b^W_i \in \mathbb{Z} \quad \forall i \in \mathcal{V}^W \tag{16}$$

$$0 \leq f^E_{i,j,t,s} \leq \bar{E}_{i,j} \quad \forall (i,j) \in \mathcal{E}^E, t \in \mathcal{T}, s \in \mathcal{S} \tag{17}$$

$$0 \leq f^G_{i,j,t,s} \leq \bar{G}_{i,j} \quad \forall (i,j) \in \mathcal{E}^G, t \in \mathcal{T}, s \in \mathcal{S} \tag{18}$$

$$0 \leq f^L_{i,j,t,s} \leq \bar{L}_{i,j} \quad \forall (i,j) \in \mathcal{E}^L, t \in \mathcal{T}, s \in \mathcal{S} \tag{19}$$

$$0 \leq s^G_{i,t,s} \leq \bar{S} \cdot y^G_i \quad \forall i \in \mathcal{V}^E, t \in \mathcal{T}, s \in \mathcal{S} \tag{20}$$

$$0 \leq s^L_{i,t,s} \leq \bar{T} \cdot y^L_i \quad \forall i \in \mathcal{V}^T, t \in \mathcal{T}, s \in \mathcal{S} \tag{21}$$

$$0 \leq c^G_{i,t,s}, d^G_{i,t,s} \leq \bar{S}^G \cdot y^G_i \qquad \forall i \in \mathcal{V}^E, t \in \mathcal{T}, s \in \mathcal{S} \tag{22}$$

$$0 \leq c^L_{i,t,s}, d^L_{i,t,s} \leq \bar{S}^L \cdot y^L_i \qquad \forall i \in \mathcal{V}^E, t \in \mathcal{T}, s \in \mathcal{S} \tag{23}$$

$$u^E_{i,t,s} \geq 0 \qquad \forall i \in \mathcal{V}^I \cup \mathcal{V}^R, t \in \mathcal{T}, s \in \mathcal{S} \tag{24}$$

$$u^G_{i,t,s} \geq 0 \qquad \forall i \in \mathcal{V}^I, t \in \mathcal{T}, s \in \mathcal{S} \tag{25}$$

$$y^G_i \in \mathbb{Z} \qquad \forall i \in \mathcal{V}^E \tag{26}$$

$$y^L_i \in \mathbb{Z} \qquad \forall i \in \mathcal{V}^T \tag{27}$$

All in all, our 2-stage stochastic mixed-integer linear model is given by:

$$\min_{\substack{b^S_i, b^W_i, z^S_i, z^W_i \\ f^E_{i,j,t,s}, f^G_{i,j,t,s}, f^L_{i,j,t,s}, g_{i,t,s}, u^E_{i,t,s}, u^G_{i,t,s}, \\ s^L_{i,t,s}, c^L_{i,t,s}, c^L_{i,t,s}, s^G_{i,t,s}, c^G_{i,t,s}, d^G_{i,t,s}}} (1) + (2)$$

$$\text{s.t.} \quad (3) - (27)$$

Note that we do not consider complementarity constraints between the charge and discharge variables of the storage systems ($c^G_{i,t-1,s}$ and $d^G_{i,t-1,s}$, $c^L_{i,t-1,s}$ and $d^L_{i,t-1,s}$). In fact, charging and discharging a storage system in the same time period is not optimal because of the inefficiencies in these systems.

Finally, we also assume that there is no wear and tear on equipment and that the efficiencies of the technologies and processes do not deteriorate over time. Our investigation also indicated that the cost of installing renewables was mostly variable; this is dependent on the number of turbines/panels installed. Therefore, we do not consider one-off setup costs for this investment.

2.2 Data Input

Through the input of data parameters that describe different realities (e.g. cities, climates, costs), the model presented in Section 2.1 can be utilized to study the viability of green hydrogen for various contexts. In this section, we provide a brief overview of how we build the data instances used in the computational experiments in Section 3. Graphs that visualize the data instance described in this section can be found on the interface as described in Section 2.3.

We have considered standard data units in our instances and measured electricity in MW, gas and liquid hydrogen in kg, and money in US $. For the parameters (and variables) concerning the dimensions of renewable plants, the minimum units are one row with 100 panels for solar plants and one wind turbine for wind plants.

We design a network of 12 locations. According to the data provided, we consider 5 residential areas, 2 industrial areas, 2 candidate renewable plant locations (one solar and one wind), and 3 locations with an electrolyzer, liquid tank, and fuel cell technologies, respectively. We consider 4 days representative of the 4 quarters in a year, and each day is subdivided into 96 15-minute time periods. Note that all possible lines between locations according to our network scheme in Figure 1 are present in the data instance.

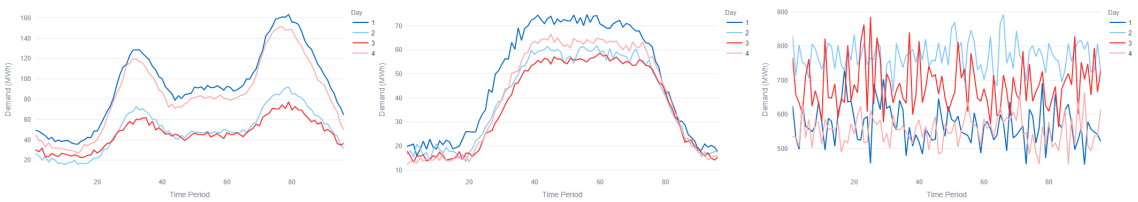

(a) Residential Electricity. (b) Industrial Electricity. (c) Industrial Gas.

Figure 2: Total Network Demand.

Some data parameters were provided by the competition organizers in the problem description. Namely, the investment costs in solar PV panels B_i^S and wind turbines B_i^W, the electricity $(D_{i,t}^E)$ and gas $(D_{i,t}^G)$ demand of 5 residential and 2 industrial areas. The total demand of these areas for electricity and gas is presented in Figure 2.

In addition, an average scenario of renewable generation $G_{i,t,s}^S$, $G_{i,t,s}^W$ is also provided. We consider 9 scenarios by combining low, medium, and high cases for both solar and wind. We build the generation data for the remaining scenarios by considering deviations of +20% and -20% from the given (medium) scenario as depicted in Figure 3 and Figure 4. Note that we consider in-shore

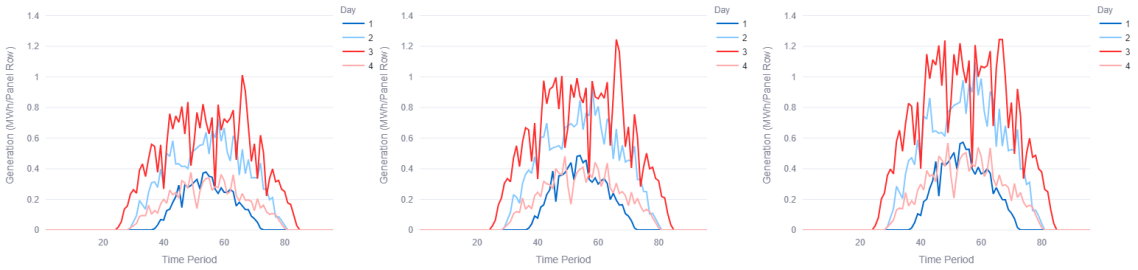

(a) Low Scenario. (b) Medium Scenario. (c) High Scenario.

Figure 3: Solar Generation.

wind generation, but by adapting these inputs, the model would be suitable to study off-shore wind potential as well. These scenarios have different weights w_s in the operational costs of the

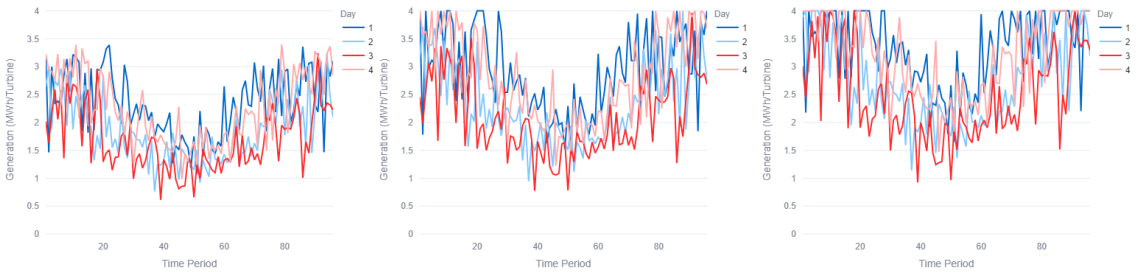

(a) Low Scenario. (b) Medium Scenario. (c) High Scenario.

Figure 4: Wind Generation.

objective function as depicted in Figure 5. The values were chosen by assigning the likeliness of

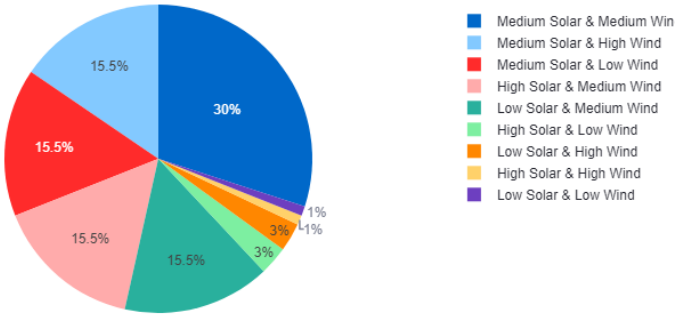

Figure 5: Scenario Weights.

the scenarios in real life where an average scenario is more probable than the extremes. Therefore, the medium solar and medium wind scenario has the biggest probability with 30%, then a 15.5% for all the other combinations with a medium, 3% for the mix of high and low solar and wind, and 1% for the low/low and high/high scenarios, which should be less likely to occur.

Next, we detail the remaining costs. We set the cost of intraday gas storage B_i^G at \$20,000 per storage system where each storage system has a maximum capacity $\bar{T}$ of 9kg [2]. Similarly, the cost of long-term liquid hydrogen tanks is \$800,000 per tank, and tanks have a maximum capacity $\bar{S}$ of 4,000kg [1]. Moreover, we set the operational costs of the intraday gas storage C^G at \$10/kg [13, 9], and those of the long-term liquid tanks C^L at \$0.2/kg [3].

The efficiencies of the electrolysis process at electrolyzers $\eta_i^E$and of the gasification process at fuel cells η_i^F are provided in the problem description as 70% and 75%, respectively. For the hydrogen tank, we assume the gasification process is entirely efficient with an efficiency of 100%. For the efficiencies associated with the storage technologies, we consider both self-discharge rates α_i^G and α_i^L to be 1.5%, the charging and discharging efficiencies of intraday gas storage to be 70% and those of long-term liquid storage to be 75%.

We allow for a maximum loss of load of 3.5% for both electricity L^E and gas L^G, which is equivalent to 3 hours per year. In addition, we consider a maximum capacity $\bar{P}_i$ of 5,000 rows of 100 panels corresponding to a solar plant of 1 km^2, and a maximum capacity $\bar{W}_i$ of 100 turbines corresponding to a wind farm of 50km^2. We assume that the lines between two locations in our network have a maximum capacity of 500MW for electricity lines $\bar{E}_{i,j}$, 100,000kg for hydrogen gas lines $\bar{G}_{i,j}$ [8], or 500,000kg for liquid hydrogen lines $\bar{L}_{i,j}$.

Finally, according to the problem description, we consider that 1MW of electricity corresponds to 0.05kg of gas (U^{EG}), and 1kg of hydrogen gas is equivalent to 1kg of liquid hydrogen (U^{GL}).

2.3 User Interface

In order to simplify the interaction of decision-makers with our optimization model and allow them to use the model's solutions to extract practical insights to inform their decisions, we have implemented a user interface. This interface can be accessed in the following URL: `https://hydrogenius-edinborgh-mopta24.streamlit.app/`.

This interface allows the user to personalize the data as needed in the *Data Input* page and visualize it in the *Data Visualization* page. The default instance which we consider in this report and which we detail in Section 2.2 is also directly available on these pages. In addition, the user can visualize the model's solution for the data input provided in the *Solution Visualization* page. This allows the user to try out different data inputs and see how they affect the solution.

This interface can alternatively be run locally by downloading the contents of the following GitHub repository which hosts it: HYDROGENius-EdinbORgh_MOPTA24.git.

3 Results & Discussion

In this section, we present the computational results obtained from our model's solution and discuss their significance to the study of the viability of green hydrogen.

3.1 Solution Analysis of Minimum Non-trivial Case

In this section, we discuss the solution of our optimization model given the 12-location network data described in Section 2.2.

This instance results in a total cost of circa \$251 Million, given that around \$250 Million results from investment costs, and the \$443 Thousand in operational costs for the 4 days representative of the 4 quarters. The solution consists of building 3 rows of 100 solar PV panels each, 78 wind turbines, and 19 liquid hydrogen storage tanks. At the optimal solution, no intraday gas storage is invested in.

When looking at the investment costs per technology type (solar, wind, hydrogen gas, and liquid hydrogen storages) in Figure 6, we notice that the majority of costs come from an investment in wind turbines, with the second most relevant investment being the liquid hydrogen storage. When considering the approximate operational costs per scenario in Table 1, we can see that the wind

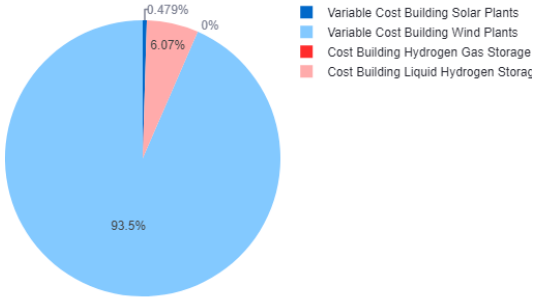

Figure 6: Investment Costs - Breakdown per Technology.

Wind Scenario	Operational Cost (Thousands of US $)
High	5
Medium	102-109
Low	2000

Table 1: Approximate Operational Costs - Breakdown per Scenario.

scenarios are the ones with the highest impact on the operational costs. In other words, scenarios with low wind generation result in significantly higher operational costs of storage systems. This is coherent with the fact that the model has chosen to invest in a large wind plant and a small solar plant to offer some flexibility.

We can also see the high impact of the wind scenario in other parts of the solution, such as the amount of renewable electricity spilled and the use of liquid hydrogen tank storage.

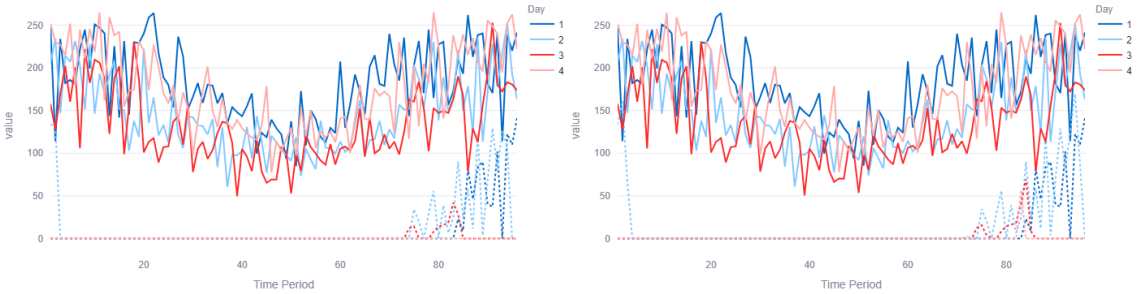

(a) Low Solar & Low Wind.

(b) High Solar & Low Wind.

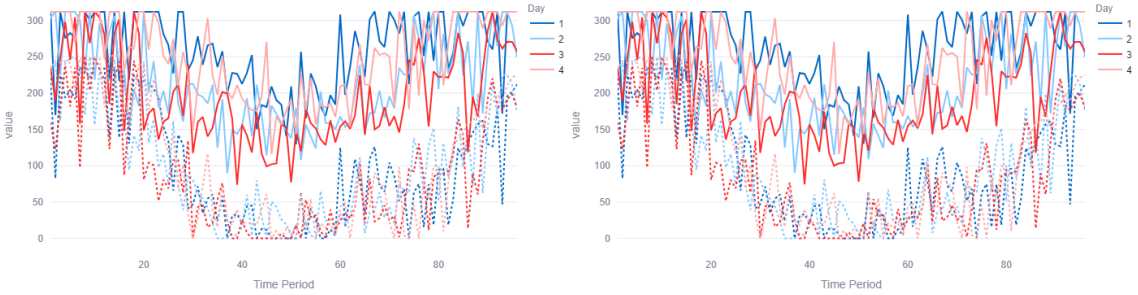

(c) Low Solar & High Wind.

(d) High Solar & High Wind.

Figure 7: Electricity Generation (continuous lines) and Electricity Spillage (dotted lines).

In Figure 7, we can confirm that under scenarios with similar wind, the spillage is similar independently of solar generation being high or low. While in scenarios with low wind, there is little spillage, which mostly occurs at the end of the day, in scenarios where there is a lot of wind generation, renewable electricity is spilled in more periods of the day and in higher amounts.

A similar pattern can be observed when investigating how liquid hydrogen storage is used and managed throughout the time horizon. In Figure 8, we present the storage level of the liquid

hydrogen tank for the 3 wind scenarios and for the medium solar generation scenario. Note that similar patterns will be observed for high and low solar generation, once again depicting that the solar generation scenarios do not have as big of an impact as the wind generation ones do.

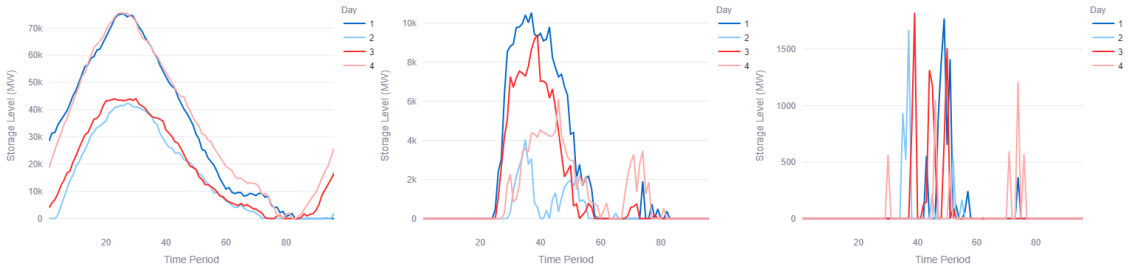

(a) Low Wind. (b) Medium Wind. (c) High Wind.

Figure 8: State-of-charge of Liquid Hydrogen Tank Storage.

On the one hand, when wind generation is low (Figure 8a), the storage is more carefully managed to leverage the generation at the start of the day to meet the peak of electricity demand between time periods 25 and 85 (see Figure 2a and Figure 2b). On the other hand, when wind generation is high (Figure 8c), the storage is only used more sporadically, and the state-of-charge is orders of magnitude lower. These observations attest that Hydrogen storage has a clearer value for the network when renewable generation is lower.

Finally, we note that the loss of load constraints for both electricity (5) and gas (6) are active under every scenario. This is expected as operational costs can be reduced by not meeting demand, even if the same investment needs to be made initially. We discuss this theme further in Section 3.2, where we study the shadow prices of these constraints and how the optimal objective cost changes with different values of maximum loss of load allowed.

3.2 Economics of the Loss of Load

For a green-hydrogen-powered grid to become a reality, one may need to buy non-renewable energy during the investment stages while hydrogen systems and renewable plants are being built, or as a back-up energy source for extreme, unfavorable scenarios. However, in the long-run, for renewable energy and green hydrogen to be viable, their prices will have to be comparable and competitive with those of non-renewable energy.

In Section 3.1, we alluded to the fact that the loss of load bounding constraints (5) for electricity and (6) for gas remain active in the solutions found. In this section, we consider that same data instance and study the shadow prices (or dual values) associated with those constraints. These shadow prices provide information on how much one would be willing to pay for being allowed one additional unit (MW) of loss of load. In other words, they represent the price that we would be willing to pay for non-renewable energy. Consequently, for a green-hydrogen-powered grid to have practical potential, we would like to verify shadow prices comparable to current energy prices.

Throughout this section, we present computational results that we obtain by solving our model over a grid of values of loss of load for electricity and gas. Since our model is a mixed-integer linear model, we take the following steps to obtain shadow prices for the loss of load constraints. First, we fix the integer investment decision variables (b_i^S, b_i^W, y_i^G, y_i^L) at their optimal values. Then, we solve the remaining linear model to compute the shadow prices associated with constraints (5) and (6). Note that these shadow prices are only valid while the integer solution, which is fixed, remains optimal.

Before discussing how the shadow prices vary over this grid, we show the total expected operational costs for these different losses of loads percentages in Figure 9. As expected, Figure 9 reveals that the smaller the levels of loss of load allowed, the higher the operational costs. We note that the difference in the total operational costs between allowing 0% loss of load for electricity and 1.5% is over $2,000,000. It is also possible to observe that changes in the percentage of loss of

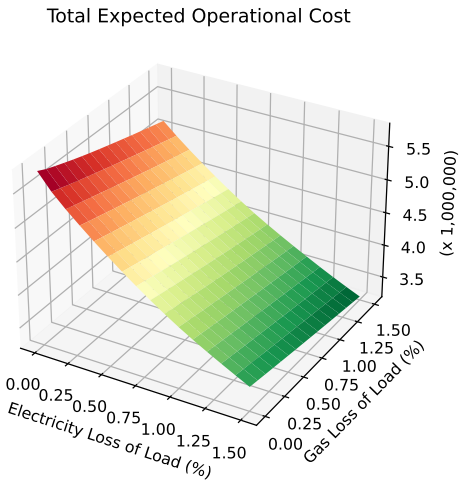

Figure 9: Total expected operational cost for a grid of loss of load percentages for electricity and gas.

load for electricity have a much greater impact on the expected operational costs than changes in the gas loss of load.

In Figure 10, we can see the shadow prices for loss of electricity load (10a) and of gas load (10b). We observe that the shadow prices for the loss of gas load are smaller both in range and in

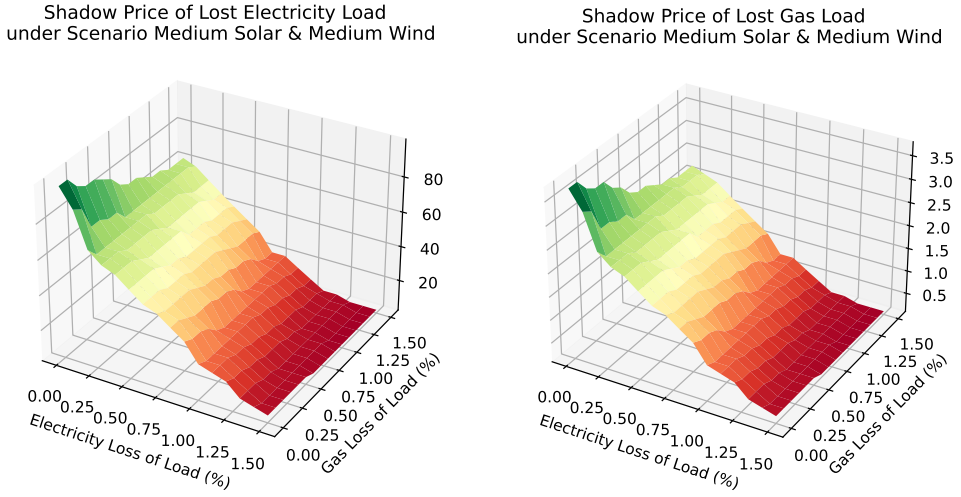

(a) Electricity.

(b) Gas.

Figure 10: Loss of Load Shadow Prices under the scenario with Medium Solar and Wind.

value than those of electricity load. This confirms what we noticed in Figure 9 that the electricity loss of load is more valuable than that of gas; this is it has a greater impact on the operational costs.

Throughout the rest of this section, we focus on the loss of electricity load shadow prices and compare its behavior under different renewable generation scenarios. In Figure 11, we show how the behavior of the shadow prices of loss of electricity load changes with changes in wind generation (under the same solar generation scenario). We can see that the graphs 11a and 11b are significantly different in the range of shadow prices they present. As expected, when there is more wind generation (Figure 11b), the shadow prices are smaller as we are willing to pay less

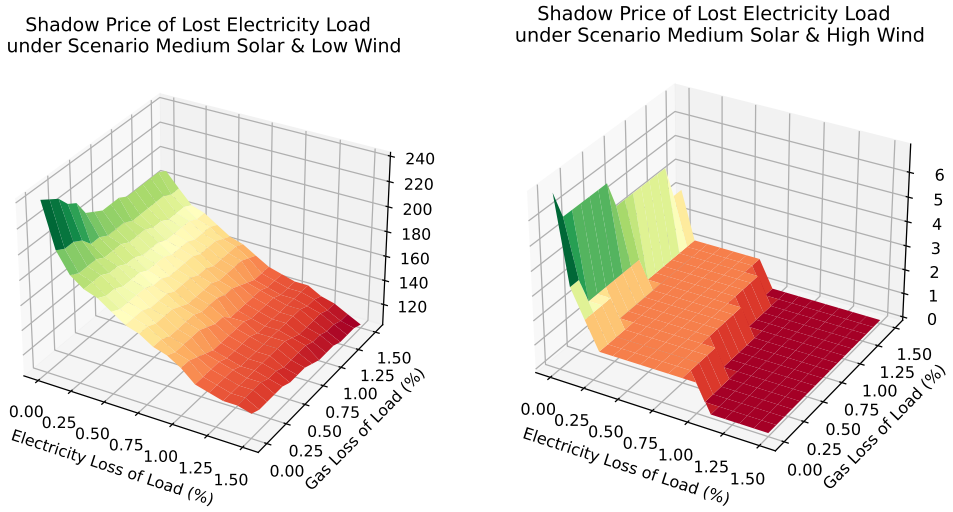

(a) Low Wind.

(b) High Wind.

Figure 11: Electricity loss of load shadow prices of constraint (5) under scenarios with medium solar generation.

for losing load as our generation is abundant. When wind generation is low, the shadow prices increase as meeting demand in this case is more difficult in this case and being able to lose more load results in higher savings.

In Figure 12, we show these same changes are not as noticeable when we change the solar generation instead (under the same wind generation scenario). In fact, the two graphs 12a and 12b look fairly similar. This is once again coherent with the model's decision to invest in a large

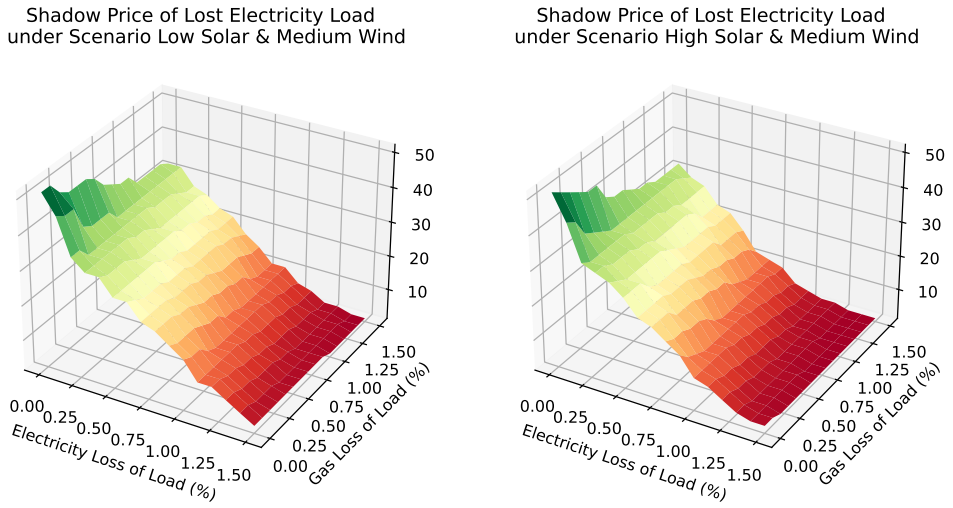

(a) Low Solar.

(b) High Solar.

Figure 12: Electricity loss of load shadow prices of constraint (5) under scenarios with medium wind generation.

wind plant, but only a small solar plant. Note that the scenario weights are not causing these differences in the influence of wind and solar, as they are created to be symmetrical with respect to wind and solar as seen in Figure 5.

3.3 Green Hydrogen Viability

In this section, we discuss how the shadow prices for the loss of electricity load compare with current electricity prices in the USA, and what that says about the viability of green hydrogen.

Considering the data instance detailed in Section 2.2, where the percentage of loss of electricity load is 0.035%, we obtain the shadow prices in Table 2. In this same instance, the total electricity

Solar Scenario	**Wind Scenario**	**Shadow Price ($)**
Medium	Medium	99.16
Medium	High	5.77
Medium	Low	240.06
High	Medium	49.36
High	High	0.37
High	Low	46.46
Low	Medium	51.23
Low	High	1.12
Low	Low	15.49

Table 2: Electricity shadow prices for a loss of electricity load of 0.035% under each scenario

demand (overall load locations and time periods) is 10,522.30 MWh, and hence the maximum loss of electricity load is 3.68 MWh.

If we consider instead a loss of load of 0.0326241%, which translates into 1MW less of loss of load, similar to the interpretation of shadow prices, we would be able to lose 3.43 MWh of load. In other words, we would have to lose 0.25 MWh less of load. Assuming the average electricity rate in the USA of $161/MWh [6], buying these 0.25 MWh of load from the grid would cost $40.25.

When the cost of non-renewable energy $40.25 is smaller than the shadow price in Table 2, which is the price we would be willing to pay for buying that energy elsewhere (or in other words, the savings in operational costs we obtain from being able to lose that extra load), then it would be more profitable to buy non-renewable energy, and green-hydrogen would not desirable.

We can observe that in the scenarios with high wind, this is the case. Since a big investment in wind is made in the optimal solution, then when wind is high we are not willing to pay too much for losing electricity load. Consequently, green hydrogen becomes the more profitable source of energy. In other scenarios, this is not the case, which shows that under the current technology and energy prices considered in our input data, in these scenarios, green hydrogen would be more costly than non-renewable energy.

If we have an electricity price of $105/MWh on the lower end of the spectrum (like in North Dakota [6]), then the same conclusions still hold. If instead we have a higher electricity price of $439.3/MWh (like in Hawaii [6]), then green hydrogen becomes the more profitable option in almost all the scenarios.

Finally, the user interface discussed in Section 2.3 can be used to better investigate different case studies by adjusting the investment and operational costs, generation scenarios, and respective weights so that a similar analysis can be conducted for different regulatory and weather realities.

3.4 Sensitivity Analysis for Trends in Future Investment Costs

The strategic decisions of investment in renewable and storage technologies are made over multiple years. Therefore, it is important to confirm that the solution obtained is robust to an increase or decrease in their investment costs (B_i^S, B_i^W, B_i^G, B_i^L). In this section, we run a computational experiment to evaluate how robust the optimal solution is to changes in these technologies' costs.

In order to do so, we assume that the investment is to be concluded by 2050. We assume that electricity demand will increase 1% per year [5], i.e., by 2050, the total demand will have increased by 28.24%. We consider the instance as detailed in Section 3.1 where the demand per time period and the maximum building capacities of generation and storage technologies reveal this increase in 28.24%.

We conduct a type of sensitivity analysis on our mixed-integer two-stage stochastic problem by changing the investment cost coefficients in the objective function, and evaluating the optimal solution and value for each possible investment cost change.

In this new instance with increased electricity demand, the optimal solution is to build 98 wind turbines (20 more than in the previous solution in Section 3.1) and 24 liquid hydrogen storage tanks (5 more than in the previous solution). Unlike in the previous solution, in this case no rows of solar PV panels are built.

In the next sections, we show the results from this experiment by varying the investment costs: first one at a time in Section 3.4.1 and then by changing both the wind and solar investment costs simultaneously in Section 3.4.2.

3.4.1 Univariate Analysis

In Figure 13, we can see the optimal number of wind turbines, rows of PV Panels and H2 gas and liquid storages for different percentage increases or decreases in the investment cost of wind turbines (13a), rows of solar panels (13b), H2 liquid tanks (13c) or H2 intraday gas storage (13d). For example, the values -50 and 50 in the x-axis of Figure 13a represent a 50% decrease and a 50% increase in the investment cost of wind turbines (B_i^W), respectively.

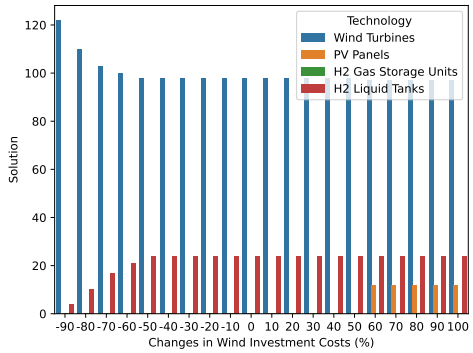

(a) Changing Wind Turbines Cost.

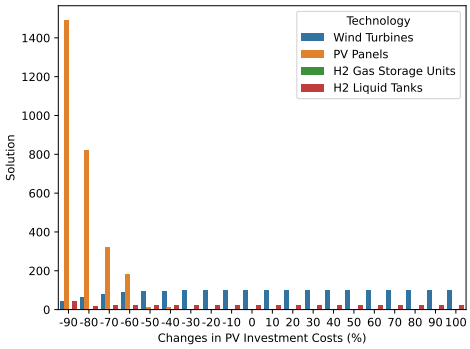

(b) Changing PV Panels Cost.

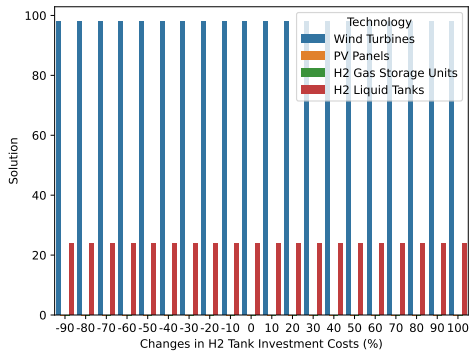

(c) Changing H2 Liquid Tanks Cost.

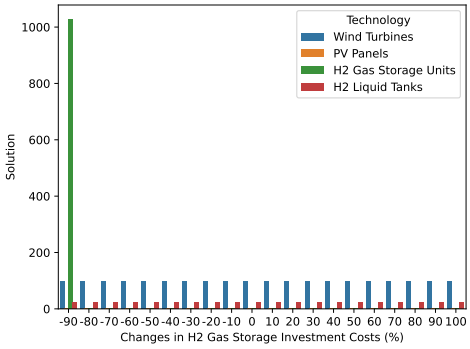

(d) Changing Intraday H2 Gas Storage Cost.

Figure 13: Optimal Solution for changes in investment costs.

In Figure 13c and Figure 13d, we can observe that changes in the investment costs of H2 liquid tanks and H2 gas storage systems do not have an impact on the optimal solution unless drastic decreases occur in the costs of these storage technologies.

In Figure 13a, we can observe that as long as wind turbine investment costs do not decrease or increase by over 50%, the same solution holds optimal. When these costs decrease significantly, we see the solution tending towards building an excessive number of wind turbines to always meet demand from generation and hence avoid building storage systems to provide time-shifting

of generation. While this solution is reasonable, given the extreme decrease in wind turbine costs, it would not be a very resilient solution. In the scenario where wind turbine costs increase by over 50%, we can also see the solution changing to build more solar PV generation instead. This is coherent with the wind cost increase, as this makes PV solar a financially more attractive investment.

In Figure 13b, we can observe that as long as PV panel investment costs do not decrease by over 50%, the same solution is optimal. For decreases in solar generation technology costs of over 50%, we can see that the number of PV panels to be built at the optimal solution quickly increases while a small decrease in the number of wind turbines invested in takes place, while the long term liquid storage increases to account for the possible power outages.

3.4.2 Bivariate Analysis (Wind & Solar)

Given that renewable generation investment costs are the ones revealed to have a greater impact on the optimal solution in Section 3.4.1, in this section, we evaluate how the solution and objective value change for simultaneous changes in wind and solar costs.

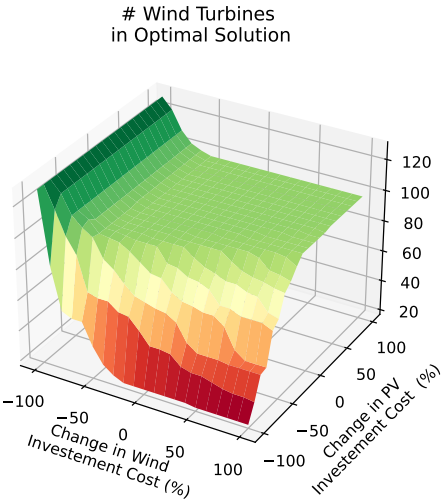

(a) Number of Wind Turbines.

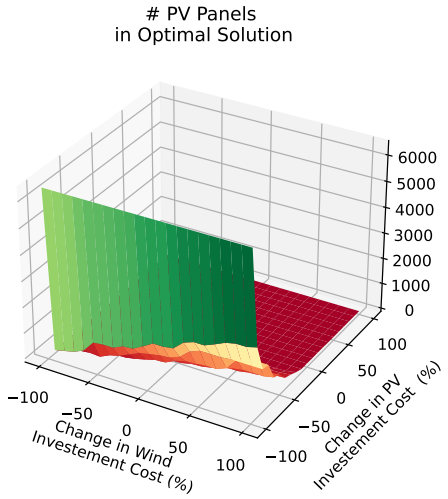

(b) Number of rows of PV Panels.

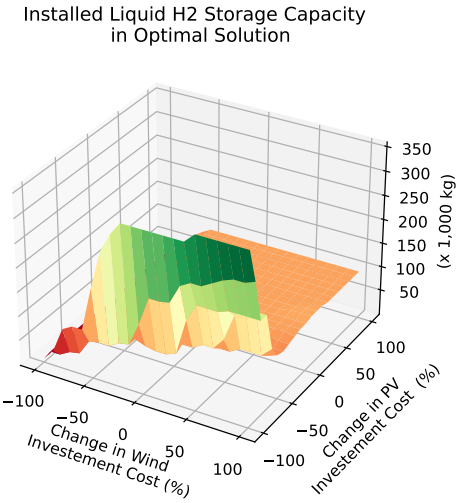

(c) Installed Capacity of H2 Liquid Tanks.

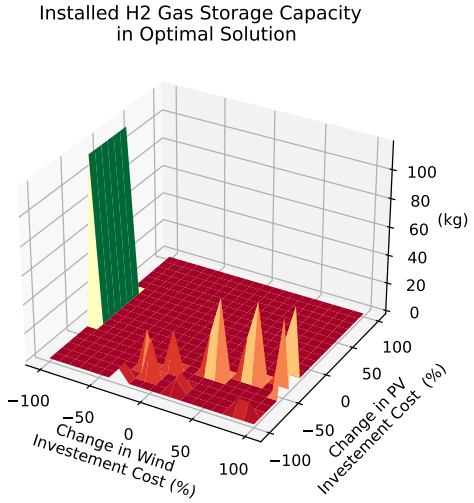

(d) Installed Capacity of H2 Gas Storage Units.

Figure 14: Optimal Solution for changes of wind and solar investment costs.

In Figure 14, we present the optimal solution, namely the number of wind turbines (14a) and the number of rows (of 100) solar PV panels (14b), and the total installed capacity of liquid hydrogen tanks (14c) and hydrogen gas storage (14d). The capacity values in Figure 14c correspond to between 0 and 80 liquid storage tanks of capacity 4000kg each, and in Figure 14d to 0 and 12 hydrogen gas storage units of capacity 9kg each.

We can observe that the number of wind turbines in Figure 14a and the number of rows of solar panels Figure 14b are complementary. At the original investment costs, our solution privileges building wind turbines over solar PV panels. As the solar costs decrease, there is a bigger investment in solar panels, and simultaneously, fewer wind turbines are built.

A similar phenomenon can be observed in the plots of the optimal hydrogen storage capacity in which the peaks (orange and green) in Figure 14d match the steps in Figure 14c. In other words, these peaks represent boundary points where more storage is needed but where an extra liquid tank would not yet be financially profitable. In this case, the model opts for bridging that extra bit of storage needed with the smaller intraday gas storage systems. Note that this explanation is also consistent with the significantly different z-axis scales of these two plots.

Finally, the increase in the number of liquid hydrogen tanks (14c) with the decrease in the solar investment costs is consistent with the trends in the investment in renewables technologies. As solar investment costs decrease, more solar PV panels (14b) and fewer wind turbines (14a) are built. Since solar generation is dependent on sunlight and hence nonexistent for long periods overnight, the need to invest in storage systems to shift the energy generated to meet demand at all time periods increases. Hence, as solar investment costs decrease, the installed capacity of liquid hydrogen tanks (14c) increases.

In Figure 15, we present the total investment and operational costs for the same ranges of wind and solar investment costs.

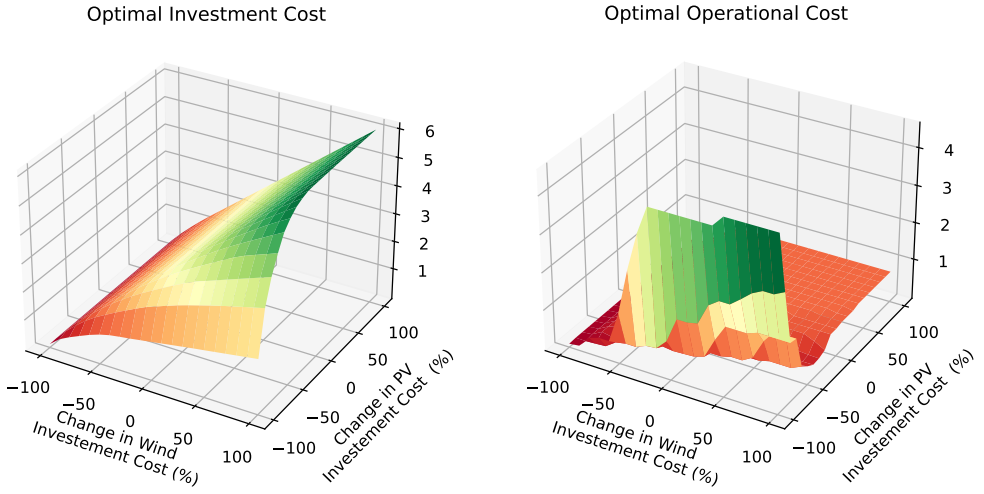

(a) Investment Cost ($\times\$10^8$). (b) Operational Cost ($\times\$10^7$).

Figure 15: Optimal Costs for changes of wind and solar investment costs.

In Figure 15a, we can observe that the total investment cost increases with the increase in solar and wind investment costs, as was expected. Figure 15b shows the expected operational costs increase with the higher number of solar generation and reduced number of wind generation, since these lead to a greater need to use the storage systems to shift generation to meet demand as previously discussed.

In conclusion, we have seen that our model is robust to changes in the investment costs, for the data collected. Decision makers can conduct a similar analysis to adjust the solution to be implemented to their predictions of the cost trends and evaluate how robust that solution is to unexpected investment cost changes.

Current predictions state that the PV costs will decrease by about 50% by 2030 [16] and that

the wind costs will fall by at least 37% by 2050 [18]. If a decision maker were to rely on these predictions (and assume that the hydrogen storage costs remain the same) for their investment decisions, the same optimal solution would be valid and robust to these cost changes.

4 Conclusion

In this section, we briefly summarize the most relevant findings of our report and detail how this work could be further improved in future work.

4.1 Key findings

All in all, the results in this report show that there is potential for green hydrogen as a source of baseload support in the transition to a fully renewable-powered energy grid.

For the data considered, we see that a fully-renewable network driven by green hydrogen has a greater potential to succeed under realities where wind generation is high. In addition, we note that the main driver for the potential and profitability of green hydrogen lies in the electricity demand and prices, as opposed to those for gas. We also conclude that the investment in long-term liquid hydrogen storage is more valuable for taking full advantage of hydrogen as a baseload source than that in shorter-term intraday hydrogen gas storage. Finally, we have seen that our model is robust to changes in the investment costs for the data collected, which is particularly relevant for future case scenarios when costs could vary significantly depending on the technology advances.

4.2 Future Improvements

The approach presented in this report has further potential to bring valuable insights to the adoption of green hydrogen. In this section, we suggest some directions for future work.

First, uncertainties in the model could be further explored. One could consider a larger or more relevant set of renewable generation scenarios by developing a more accurate generation forecast based on weather data and different locations. Alternatively, other sources of uncertainty could be considered, such as residential demand patterns or technology investment costs.

Moreover, we could extend the optimization model developed to detail other aspects of the grid's operation. For example, we could account for the economy of scale in prices when designing the objective function and its cost parameters or for the impact of ramping in charging and discharging of intraday gas storage by modeling the corresponding constraints.

This study would allow us to suggest policy changes that would address the main obstacles that green hydrogen faces today by allowing us to identify which components would have to become cheaper to make green hydrogen more desirable economically. Alternatively, we could better account for a long time horizon of investments. For example, by computing the net discounted present value of the investments or by allowing for an initial setup to be installed already. In other words, assume that some renewable plants and hydrogen storage systems are already built. From a modeling perspective, this can be achieved by enforcing lower bounds on the corresponding investment variables.

References

[1] Creo International, *Creo International Products*. `https://creouk.com/products/`, accessed on 19-04-2024.

[2] Cryolor, *Liquid hydrogen storage*. `https://www.cryolor.com/cryogenic-storage-tanks/liquid-hydrogen-storage`, accessed on 19-04-2024.

[3] Department for Energy Security & Net Zero, *Hydrogen Transport and Storage Cost Report*, tech. rep., UK Government, 2023. `https://www.gov.uk/government/publications/hydrogen-transport-and-storage-cost`.

[4] T. Egeland-Eriksen, A. Hajizadeh, and S. Sartori, *Hydrogen-based systems for integration of renewable energy in power systems: Achievements and perspectives*, International Journal of Hydrogen Energy, 46 (2021), pp. 31963–31983.

[5] EIA U.S. Energy Information and Administration, *Electricity demand grows at a modest rate throughout the projection period.* https://www.eia.gov/outlooks/aeo/electricity/sub-topic-01.php, accessed on 24-06-2024.

[6] EnergyBot, *Electricity Rates By State.* https://www.energybot.com/electricity-rates/, accessed on 14-05-2024.

[7] M. Fochesato, P. Heer, and J. Lygeros, *Multi-objective optimization of a power-to-hydrogen system for mobility via two-stage stochastic programming*, 2042 (2021), p. 012034 (6 pp.). Presented at the CISBAT 2021, Lausanne, Switzerland, September 8-10, 2021.

[8] GERN, *Determining Energy Capacity for H2 in existing NG pipelines - Summary Report, November 2023*, tech. rep., GERN, 2023. https://www.gerg.eu/wp-content/uploads/2022/07/GERG-Energy-Capacity-final-publishable-summary.pdf.

[9] B. Ghorbani, S. Zendehboudi, N. M. C. Saady, and M. B. Dusseault, *Hydrogen storage in north america: Status, prospects, and challenges*, Journal of Environmental Chemical Engineering, 11 (2023), p. 109957.

[10] Y.-H. Huang, J.-H. Wu, and Y.-J. Hsu, *Two-stage stochastic programming model for the regional-scale electricity planning under demand uncertainty*, Energy, 116 (2016), pp. 1145–1157.

[11] D. J. Jovan and G. Dolanc, *Can green hydrogen production be economically viable under current market conditions*, Energies, 13 (2020).

[12] G. Mavromatidis, K. Orehounig, and J. Carmeliet, *Design of distributed energy systems under uncertainty: A two-stage stochastic programming approach*, Applied Energy, 222 (2018), pp. 932–950.

[13] C. Moran, P. Deane, S. Yousefian, and R. F. Monaghan, *The hydrogen storage challenge: Does storage method and size affect the cost and operational flexibility of hydrogen supply chains?*, International Journal of Hydrogen Energy, 52 (2024), pp. 1090–1100.

[14] A. Rezaee Jordehi, S. A. Mansouri, M. Tostado-Véliz, M. Carrión, M. Hossain, and F. Jurado, *A risk-averse two-stage stochastic model for optimal participation of hydrogen fuel stations in electricity markets*, International Journal of Hydrogen Energy, 49 (2024), pp. 188–201.

[15] A. H. Schrotenboer, A. A. Veenstra, M. A. uit het Broek, and E. Ursavas, *A green hydrogen energy system: Optimal control strategies for integrated hydrogen storage and power generation with wind energy*, Renewable and Sustainable Energy Reviews, 168 (2022), p. 112744.

[16] Uwe Dahlmeier, *Empirical approach shows PV is getting cheaper than all the forecasters expect.* PV Magazine, December 2023. https://www.pv-magazine.com/2023/12/05/empirical-approach-shows-pv-is-getting-cheaper-than-all-the-forecasters-expect/, accessed on 24-06-2024.

[17] L. Valverde-Isorna, D. Ali, D. Hogg, and M. Abdel-Wahab, *Modelling the performance of wind–hydrogen energy systems: Case study the hydrogen office in scotland/uk*, Renewable and Sustainable Energy Reviews, 53 (2016), pp. 1313–1332.

[18] R. Wiser, J. Rand, J. Seel, P. Beiter, E. Baker, E. Lantz, and P. Gilman, *Expert elicitation survey predicts 37% to 49% declines in wind energy costs by 2050*, Nature Energy, 6 (2021), pp. 555–565.

[19] M. Yue, H. Lambert, E. Pahon, R. Roche, S. Jemei, and D. Hissel, *Hydrogen energy systems: A critical review of technologies, applications, trends and challenges*, Renewable and Sustainable Energy Reviews, 146 (2021), p. 111180.

A Notation

In this appendix, we present Table 3, Table 4 and Table 5, which summarise the notation used for sets, parameters and variables, respectively.

Table 3: List of Sets and their description.

Set	Definition
$\mathcal{V}$	Set of vertices in the energy grid.
$\mathcal{E}$	Subset of $\mathcal{V} \times \mathcal{V}$ of edges in the energy grid.
$\mathcal{T}$	Set of time periods.
$\mathcal{D}$	Set of days in the time periods.
$\mathcal{S}$	Set of renewable generation uncertainty scenarios.
$\mathcal{V}^E$	Subset of vertices where there is a hydrogen electrolyzer.
$\mathcal{V}^F$	Subset of vertices where there is a fuel cell.
$\mathcal{V}^T$	Subset of vertices where there is a insulated cryogenic tank.
$\mathcal{V}^I$	Subset of vertices where there is a industrial demand area.
$\mathcal{V}^R$	Subset of vertices where there is a residential demand area.
$\mathcal{V}^S$	Subset of candidate vertices where a solar PV plant can be built.
$\mathcal{V}^W$	Subset of candidate vertices where a wind turbine plant can be built.
$\mathcal{E}^E$	Subset of edges where electricity flows.
$\mathcal{E}^G$	Subset of edges where hydrogen gas flows.
$\mathcal{E}^L$	Subset of edges where liquid hydrogen flows.
t_d^I, t_d^F	Indexes of $\mathcal{T}$ representing the start and end of day $d \in \mathcal{D}$, respectively.

Table 4: List of Parameters, their description and units.

Parameter	Definition	Unit
B_i^S	Cost of building one solar panel at location $i \in \mathcal{V}^S$ adjusted to the time horizon $\mathcal{T}$ given an expected life-time.	£/Panel
B_i^W	Cost of building one wind turbine at location $i \in \mathcal{V}^W$ adjusted to the time horizon $\mathcal{T}$ for an expected life-time.	£/Turbine
Z_i^S	Fixed cost of setting up a solar plant at location $i \in \mathcal{V}^S$ adjusted to the time horizon $\mathcal{T}$ given an expected life-time.	£
Z_i^W	Fixed cost of setting up a wind plant at location $i \in \mathcal{V}^W$ adjusted to the time horizon $\mathcal{T}$ for an expected life-time.	£
B_i^G	Cost of building one gas storage of size $\bar{S}$ at location $i \in \mathcal{V}^E$ adjusted to the time horizon $\mathcal{T}$ given an expected life-time.	£/Storage System
B_i^L	Cost of building one liquid tank of size $\bar{T}$ at location $i \in \mathcal{V}^T$ adjusted to the time horizon $\mathcal{T}$ for an expected life-time.	£/Tank
w_s	Weight of scenario $s \in \mathcal{S}$ for the second-stage expected value objective.	%
C^G	Storage cost of hydrogen gas	£/kg
C^L	Storage cost of liquid hydrogen	£/kg
$\bar{P}_i$	Maximum number of rows of solar panels that can be built at location $i \in \mathcal{V}^S$.	Panel Rows
$\bar{W}_i$	Maximum number of wind turbines that can be built with at location $i \in \mathcal{V}^W$.	Turbines
$\bar{T}$	Standard capacity of one hydrogen liquid tank $i \in \mathcal{V}^T$.	kg
$\bar{S}$	Standard capacity of one electrolyser gas storage $i \in \mathcal{V}^E$.	kg

$\bar{E}_{i,j}$	Maximum capacity of electricity line $(i,j) \in \mathcal{E}^E$.	MW
$\bar{G}_{i,j}$	Maximum capacity of gas line $(i,j) \in \mathcal{E}^G$.	kg
$\bar{L}_{i,j}$	Maximum capacity of liquid hydrogen line $(i,j) \in \mathcal{E}^L$.	kg
L^E	Upper bound on worst case percentage total loss of electricity load arriving at vertices $i \in \mathcal{V}^I \bigcup \mathcal{V}^R$.	%
L^G	Upper bound on worst case percentage total loss of gas load arriving at vertices $i \in \mathcal{V}^I$.	%
$D^E_{i,t}$	Electricity demand at vertex $i \in \mathcal{V}^I \cup \mathcal{V}^R$.	MW
$D^G_{i,t}$	Gas demand at vertex $i \in \mathcal{V}^I$.	kg
$G^S_{i,t,s}$	Electricity generation per solar panel at location $i \in \mathcal{V}^S$ at time period $t \in \mathcal{T}$ under scenario $s \in \mathcal{S}$.	MW/Panel Row
$G^W_{i,t,s}$	Electricity generation per wind turbine at location $i \in \mathcal{V}^W$ at time period $t \in \mathcal{T}$ under scenario $s \in \mathcal{S}$.	MW/Turbine
U^{EG}	Unit conversion factor between electricity and hydrogen gas.	MW/kg
U^{GL}	Unit conversion factor between gas and liquid hydrogen.	kg/kg
α^G_i	Self-discharge rate of intraday gas storage at electrolyzer.	%
α^L_i	Self-discharge rate of liquid hydrogen tank storage.	%
η^E_i	Efficiency of electrolysis process at electrolyzer.	%
η^T_i	Efficiency of liquefaction process at liquid hydrogen tank.	%
η^F_i	Efficiency of gasification process at fuel cells.	%
γ^G_i	Charging efficiency of intraday gas storage at electrolyzer.	%
μ^G_i	Discharging efficiency of intraday gas storage at electrolyzer.	%
γ^L_i	Charging efficiency of liquid hydrogen tank storage.	%
μ^L_i	Discharging efficiency of liquid hydrogen tank storage.	%

Table 5: List of Variables, their description and units. In red, the first-stage investment variables are displayed, and in blue, the second-stage operational variables are presented.

Variable	**Definition**	**Unit**
b^S_i	Number of solar panels to be build at location $i \in \mathcal{V}^S$.	Panels
b^W_i	Number of wind turbines to be build at location $i \in \mathcal{V}^W$.	Turbines
y^G_i	Number of gas storage/electrolysers of size $\bar{S}$ to be build at location $i \in \mathcal{V}^E$.	electrolysers
y^L_i	Number of liquid storage tanks of size $\bar{T}$ to be build at location $i \in \mathcal{V}^T$.	Tanks
$f^E_{i,j,t,s}$	Flow of electricity along edge $(i,j) \in \mathcal{E}^E$ at time period $t \in \mathcal{T}$ under scenario $s \in \mathcal{S}$.	MW
$f^G_{i,j,t,s}$	Flow of hydrogen gas along edge $(i,j) \in \mathcal{E}^G$ at time period $t \in \mathcal{T}$ under scenario $s \in \mathcal{S}$.	kg
$f^L_{i,j,t,s}$	Flow of liquid hydrogen along edge $(i,j) \in \mathcal{E}^L$ at time period $t \in \mathcal{T}$ under scenario $s \in \mathcal{S}$.	kg
$u^E_{i,t,s}$	Flow of loss of electricity load arriving at vertex $i \in \mathcal{V}^I \bigcup \mathcal{V}^R$ at time period $t \in \mathcal{T}$ under scenario $s \in \mathcal{S}$.	MW
$u^G_{i,t,s}$	Flow of loss of gas load arriving at vertex $i \in \mathcal{V}^I$ at time period $t \in \mathcal{T}$ under scenario $s \in \mathcal{S}$.	kg
$g_{i,t,s}$	Renewable electricity generation at location $i \in \mathcal{V}^S \cup \mathcal{V}^W$ at time period $t \in \mathcal{T}$ under scenario $s \in \mathcal{S}$.	MW

$a_{i,t,s}$	Renewable electricity spillage at location $i \in \mathcal{V}^S \cup \mathcal{V}^W$ at time period $t \in \mathcal{T}$ under scenario $s \in \mathcal{S}$.	MW
$s^G_{i,t,s}$	Hydrogen gas stored at the intraday gas storage at vertex $i \in \mathcal{V}^E$ at time period $t \in \mathcal{T}$ under scenario $s \in \mathcal{S}$.	kg
$c^G_{i,t,s}$	Hydrogen gas charged to the intraday gas storage at vertex $i \in \mathcal{V}^E$ at time period $t \in \mathcal{T}$ under scenario $s \in \mathcal{S}$.	kg
$d^G_{i,t,s}$	Hydrogen gas discharged from the intraday gas storage at vertex $i \in \mathcal{V}^E$ at time period $t \in \mathcal{T}$ under scenario $s \in \mathcal{S}$.	kg
$s^L_{i,t,s}$	Liquid hydrogen stored at the tank storage at vertex $i \in \mathcal{V}^T$ at time period $t \in \mathcal{T}$ under scenario $s \in \mathcal{S}$.	kg
$c^L_{i,t,s}$	Liquid hydrogen charged to the tank storage at vertex $i \in \mathcal{V}^T$ at time period $t \in \mathcal{T}$ under scenario $s \in \mathcal{S}$.	kg
$d^L_{i,t,s}$	Liquid hydrogen discharged from the tank storage at vertex $i \in \mathcal{V}^T$ at time period $t \in \mathcal{T}$ under scenario $s \in \mathcal{S}$.	kg